

Fabrication and Testing of Ultra-Long Life Anode Material Using PEDOT-PSS/ Graphene Nanoplatelet Composite for Flexible Li-ion Batteries

Syed Khasim^{1,2,3,*}, Nacer Badi^{1,2}, Apsar Pasha⁴, S.A. Al-Ghamdi^{1,2}, N. Dhananjaya⁵, S. Pratibha⁵

¹ Department of Physics, Faculty of Science, University of Tabuk, Tabuk-71491, Kingdom of Saudi Arabia

² Renewable Energy Laboratory, Nanotechnology Research Unit, Faculty of Science, University of Tabuk, Tabuk-71491, Kingdom of Saudi Arabia

³ Department of Physics, PES University-Bangalore South Campus, Bangalore-560100, India

⁴ Department of Physics, Ghousia College of Engineering, Ramanagaram, Karnataka 562159, India

⁵ Centre for Advanced Materials Research Lab, Department of Physics, BMS Institute of Technology and Management, Bangalore, Karnataka 560064, India

*E-mail: syed.pes@gmail.com

Received: 11 October 2020 / Accepted: 1 December 2020 / Published: 31 December 2020

In this work, we report the fabrication of a robust, flexible and free-standing composite film electrode for Li-Ion batteries (LIBs) using a simple bar coating technique. The electrode consists of a conductive composite matrix of poly(3,4-ethylene-dioxythiophene)-poly(styrene sulfonate) (PEDOT-PSS): poly(acrylic acid) (PAA) loaded with Graphene nanoplatelets (GNPs). The successful coating of PEDOT-PSS: PAA on GNPs reduces the surface resistance and protects the electron channels on the GNPs surface from the pulverization effect during charging & discharging cycles. This PEDOT-PSS: PAA: GNPs composite electrode shows excellent cyclability with an initial reversible capacity of 1325 mAhg⁻¹ at a current density of 200 mA g⁻¹. The electrode also displays excellent capacity retention of ~83% with a coulombic efficiency of 99% after 1000 cycles. This composite structure with a porous network induces physical strains in the structure during the Lithium (Li) intake- release process, thereby increasing the interfacial contact area with organic electrolyte. Consequently, the PEDOT-PSS: PAA: GNPs composite electrodes demonstrate improved capability without capacity fading. The composite film shows an improved Young's modulus of 2.4±0.18 GPa to 4.6± 0.18 GPa and Tensile strength of 55±2.5 MPa to 78±2.5 MPa in comparison to pure PEDOT-PSS films. Benefiting from excellent conductivity, superior electrochemical performances, and mechanical flexibility, these hybrid systems could be potential materials towards the fabrication of flexible LIBs in wearable electronics.

Keywords: PEDOT-PSS, Graphene, Li-Ion, Anode, Flexible Batteries,

1. INTRODUCTION

Stretchable, flexible, and robust solid-state batteries with relatively large power densities, modest energy densities are considered to be promising sources of power supply in stretchable and wearable electronic devices. The rapid growth of wearable electronic devices has created a paradigm shift towards the development of emerging stretchable electronics that opened a new range of applications in modern electronic and energy systems. In the last few years microelectronics have experienced a tremendous advancement following the Moore's law, changing every aspect of electronics that we use in our day-to-day life. However, the conventional electronic and energy storage systems designed using brittle and hard Silicon (Si) materials are no longer viable for the modern-day applications due to limited mechanical flexibility. Recent advancement and development of flexible electronics in the last few years, witnessed a wide range of modern functional devices such as flexible transistors, smart sensors, integrated circuits, artificial/smart skin, and rolled-up display devices [1-5]. Apart from flexibility, the flexible electronics have the advantage of a low manufacturing cost for large area production due to the usage of inexpensive plastic substrates [6]. To enable electronic devices with reliable mechanical stretchability and flexibility, the modern energy storage devices like supercapacitors and batteries must be featured with light weight, incredibly compact dimensions, and improved energy/power densities with a better charge-discharge rate and long cyclic stabilities [7, 8].

Highly conductive polymers (CPs) that can store energy via redox reactions are emerging as potential materials for flexible battery applications with superior conductivity [9], light weight, and low cost fabrication [10, 11]. However, the long-time stability (longevity) of the device performance was severely affected due to the degradation of polymer structures upon cycling as a result of conformational changes in the polymer chains during the doping and de-doping processes. One of the important strategies to effectively enhance the performance of CPs is to form hybrid composite structures with mechanically robust substrates such as carbon materials which include carbon black, porous carbon, CNT's, carbon spheres, graphene, and graphene oxides [12-20]. Graphene, a well-known material consisting of a 2D arrangement of carbon atoms with superior electrical conduction, better aspect ratio in terms of surface area, excellent chemical and thermal stability, [21, 22] is known to be a promising material for energy storage and conversion applications [23]. However, carbon reacts with LiO₂ to form LiCO₃ when charged at high voltages and facilitates the decomposition of the electrolyte charging-discharging process [24-27]. The carbon surface modification in recent past emerged as a promising strategy towards preventing the carbon instability in Li-ion battery electrodes without significant capacity reduction [28]. Stable conducting polymer coatings on a carbon surface will likely suppress the side reactions by limiting the direct interactions with electrolyte or LiO₂. Hence, the electrodes of carbon coated with conducting polymer are expected to exhibit superior cyclic performance in comparison to bare carbon whilst also possessing better capacity than carbon free electrodes. Polyvinylidene fluoride (PVDF), one of the most extensively used binders in the preparation of electrodes, suffers severe volume expansions due to relatively bond strength [29]. N-methyl-2-pyrrolidene (NMP), another commonly used binder with a high boiling point, is found to be toxic which is not suitable for industrial production and a safe environment [29]. PEO, another commonly used binder, was found to reduce the porosity of composite electrodes, which are harmful

for electrode immersion. PAA, which is used as a binder in sulphur cathodes for Li-S batteries [29], is water soluble and is known to swell electrolytes [29]. A large number of binders have been extensively investigated in the past, yet it is difficult to meet expected outcomes using a single binder. Alternatively, using a combination of binders could be a useful strategy towards improving the electrochemical performance of Li-ion batteries.

Poly(3,4-ethylenedioxythiophene) : poly(styrene-sulfonate) (PEDOT-PSS) in the recent past emerged as promising material for organic electronics because of its excellent electronic conductivity, environmental stability, and mechanical flexibility with an ability to form composites with other materials [30, 31]. Furthermore, PEDOT-PSS exhibits excellent electrochemical redox properties in Li-air cells [32], plays an active role in redox reaction as a matrix, as well as coating material to suppress electrochemical side reactions. In addition, due to its superior adhesion properties, PEDOT-PSS can also be used as a conductive binder in the fabrication of electrodes. The higher concentration of PEDOT-PSS in a composite structure is expected to provide multiple functionalities such as high conductivity, stable coating over filler particles, a redox reaction matrix, and a conductive binder. The coating layers of conductive polymers such as PEDOT-PSS results in a higher charge rate transfer and facilitates enhanced electrochemical performance with better cyclability in battery devices.

The combination of conducting polymers (CPs) and graphene is able to effectively improve the energy storage performance of nanocomposites. These hybrid polymer nanocomposites not only possess the great advantage of individual components, but also the synergetic interaction between the individual components provides extra benefit towards tailoring the electrochemical properties. PEDOT-PSS based composites have been recently used for the preparation of Li-ion batteries, but the studies on mechanically flexible and robust batteries with low cost and high performance is need of the hour in wearable electronic devices.

In this study, we propose an effective strategy to fabricate highly robust and flexible anode materials based on conductive PEDOT-PSS: PAA: GNP composites for rechargeable Li-ion batteries achieved through a successful surface coating technique. In this design, the hierarchical structures of GNP were coated by highly conductive PEDOT-PSS to obtain the flexible nanocomposites via secondary doping of PAA. The surface morphology and structural features of the prepared composites were studied through various analytical techniques such as SEM, TEM, TGA and FTIR. The electronic properties of the flexible composites were studied through conductivity studies. The electrochemical performance of the prepared nanocomposites was analyzed as an anode material for flexible Li-ion batteries. The composite electrode investigated in this work exhibits i) improved electrochemical performances ii) excellent mechanical properties and iii) stable electrochemical performances up to 1000 cycles of operation in comparison to PEDOT-PSS: Graphene composites investigated so far.

2. EXPERIMENTAL

Graphene nanoplatelets (size < 2 μm , surface area 300 m^2/g), conductive PEDOT-PSS (0.5 wt% of PEDOT: 0.8 wt% PSS aqueous dispersion), poly(acrylic acid) (PAA) [Molecular weight, M_w =

450,000], ethylene carbonate (EC), diethyl carbonate (DEC), LiPF₆, hydrophilic PVDF substrates, micron filter syringes were procured from Sigma Aldrich, India and used as received.

2.1 Preparation of PEDOT-PSS: PAA-GNPs composite electrode:

PEDOT-PSS aqueous dispersion (used as received from Sigma-Aldrich) was filtered through 0.2 µm syringe and sonicated for 2 hours. Poly(acrylic acid) (PAA) (10 vol%) was added to this aqueous dispersion of PEDOT-PSS to obtain a composite binder, which was further sonicated for an hour to obtain uniform dispersions of PEDOT-PSS and PAA. The aqueous dispersion of GNPs (in DI water) were sonicated for 30 minutes to get well dispersed GNPs and further cooled in an ice bath. These dispersions of GNPs and PEDOT-PSS: PAA (2:3 w/w ratios) were used to prepare nanocomposite solutions. These nanocomposite solutions of PEDOT-PSS: PAA with GNPs were further homogenized by sonication for 2 hour. To improve the hydrophilicity of as received PVDF substrates, they were soaked in H₂O₂ for 30 minutes, followed by washing with DI water and blowing nitrogen vapor. PVDF substrates with dimensions 5 cm x 5 cm were properly cut and used to prepare the free standing electrode films. Uniform and flexible thin films were obtained by bar coating bare PEDOT-PSS, PAA treated PEDOT-PSS and PEDOT-PSS: PAA-GNPs composite onto PVDF substrate. These films were allowed to dry in an air oven for 12 hours and annealed at 120 °C to eliminate the moisture content. Finally the films were peeled off from PVDF substrates to obtain the free standing and mechanically flexible thin films of thickness 176 ± 5 µm.

2.2 Material characterizations of the films:

The structural and morphological features of bare PEDOT-PSS and PEDOT-PSS:PAA-GNPs nanocomposite films were analyzed through various techniques. Surface morphology of the bare PEDOT-PSS and PEDOT-PSS: PAA-GNPs nanocomposites were investigated through SEM (Zeiss Ultra-60-Poland) and TEM (FEI Tecnai G2 F30). The transmittance- FTIR spectra of bare PEDOT-PSS and PEDOT-PSS/PAA-GNPs were recorded (in the range 500-4000 cm⁻¹) using FTIR spectrophotometer (Perkin Elmer Frontier-USA) in KBr medium and Nitrogen atmosphere.

2.3 Electrical conductivity of the films at room temperature:

Four probe techniques were employed to evaluate the room temperature sheet resistance (R_s) of bare PEDOT-PSS, PEDOT-PSS treated with PAA and PEDOT-PSS: PAA-GNPs composites with gold electrodes deposited on top of them. Keithley current and voltage sources (2410 source meter, London) were used to obtain the sheet resistance of the films at room temperature at 40±5 %RH as described in our previous work (33).

2.4 Electrochemical characterizations of the electrode films:

The electrochemical performances of the samples were performed using half coin cells (CR-2032) assembled in a high purity glove box filled with argon (MBraun, Unilab). The bare PEDOT-PSS and PEDOT-PSS: PAA-GNPs composite free standing films peeled off from PVDF substrates were cut into circular coin shapes discs and are punched into CR-2032 assembly, and were used as anodes. Lithium foil is used as counter and reference electrode with Celgard-2400 micro porous film as a lithium battery separator. The electrolyte dispersion was prepared by mixing 1M LiPF₆ with a mixture containing diethyl carbonate and ethylene carbonate (v/v ratio 1:1). The electrochemical rate tests and cycling performance were investigated on a multichannel battery tester (Neware BTS-610). The C-V characteristics of the electrode samples were investigated on an electrochemical workstation (Chenhua CHI-660C). All the electrochemical tests were performed at room temperature under ambient conditions.

2.5 Mechanical testing of flexible films:

Tensile tests were performed on the bare and composite films as per ASTM D638 standards. An Instron-5567 universal testing machine with a crosshead speed of 0.5 mm/min was used to study the uniaxial tensile tests of the rectangular samples (30mm x 15mm x 1.5mm), at least three samples were tested for each film. The mechanical tests such as stress-strain behavior, Young's modulus and Tensile strength were conducted at room temperature under ambient conditions.

3. RESULTS AND DISCUSSION

3.1 SEM and TEM analysis

The SEM micrographs of bare PEDOT-PSS: PAA, GNPs and PEDOT-PSS: PAA-GNPs nanocomposites were depicted in figure-1 (a-c). The SEM micrograph of PEDOT-PSS: PAA (Figure-1a) shows that, the PEDOT-PSS treated with PAA results into a homogeneous surface with the formation of micro-grains due to post-curing of polymer film. The SEM micrograph of GNPs (Figure-1b) shows a flaky sheet like morphology for GNPs. The SEM micrograph of PEDOT-PSS: PAA with GNPs (Figure-1c) shows the presence of well dispersed GNPs with a formation of macro-pores in the polymer matrix. The composite micrograph shows that, the PEDOT-PSS: PAA completely covers the GNPs. The GNPs re-stacking was prevented due to the presence of PEDOT-PSS and PAA in the nanocomposite which facilitates better electrochemical reactions due to large surface area available for interactions. The formation of a conductive network and increased pore density of the nanocomposite significantly enhances the conductivity and plays an important role in improving the electrochemical performances of the composite electrode. The TEM image reveals the presence of micro-grains in PAA treated PEDOT-PSS (Figure-2a) and a magnified TEM image of GNPs shows crumpled morphology (Figure-2b). The TEM image of nanocomposite film (Figure-2c) shows that, GNPs were completely enveloped by PEDOT-PSS: PAA with a formation of network like structure.

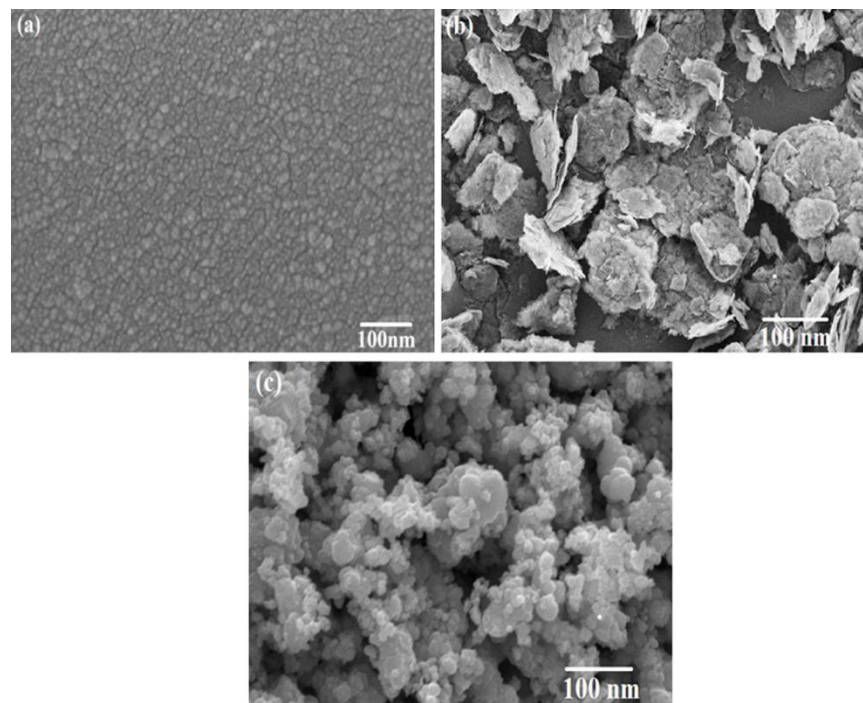


Figure 1. SEM micrographs of (a) bare PEDOT-PSS (b) bare GNPs (c) PEDOT-PSS: PAA-GNPs composite

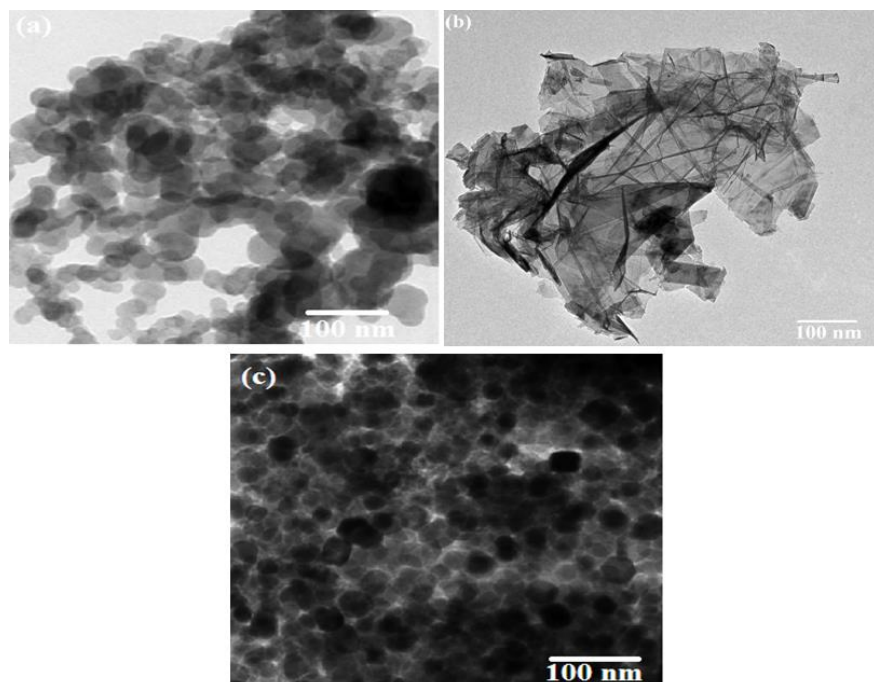


Figure 2. TEM micrographs of (a) bare PEDOT-PSS (b) bare GNPs (c) PEDOT-PSS: PAA-GNPs composite

3.2 FTIR analysis:

The structural features of bare PEDOT-PSS, GNPs and PEDOT-PSS: PAA-GNPs composites were depicted in FTIR spectra (Figure-3). The spectra of bare PEDOT-PSS exhibits characteristic bands associated with thiophene ring of PEDOT at 3500 cm^{-1} , 1620 cm^{-1} and 1380 cm^{-1} resulting from O–H, C–C and C=C stretching [34], the band due to sulphur groups of PSS appears at 1110 cm^{-1} [34]. The characteristic stretching bands of GNPs can be observed at 3490 cm^{-1} (assigned to hydroxyl group O–H stretching), 1610 cm^{-1} (C=O related to carboxylic acid and carbonyl functional groups), 1380 cm^{-1} (C–H deformation of aromatic rings) [35]. The FTIR spectra of the PEDOT-PSS: PAA-GNPs film indicates retention of important characteristic peaks of PEDOT-PSS and GNPs in composite spectra. A slight red-shift in the characteristics peaks of PEDOT-PSS and GNPs in the composite is due to delocalization of electrons arising from strong π - π interactions occurring between GNPs and the aromatic ring of PEDOT-PSS and GNPs. The band associated with stretching of C=C of quinoid ring shifts from 1620 to 1612 cm^{-1} in the composite spectra. It is worthwhile to notice that, PAA treatment transforms the benzoid structure of PEDOT-PSS matrix into quinoid structure suggests the possible conformation change of the polymer backbone chain from coil to linear structure. This effectively results in the delocalization of π -electrons contributing to highly conducting PEDOT-PSS: PAA-GNPs film with improved charge carrier mobility.

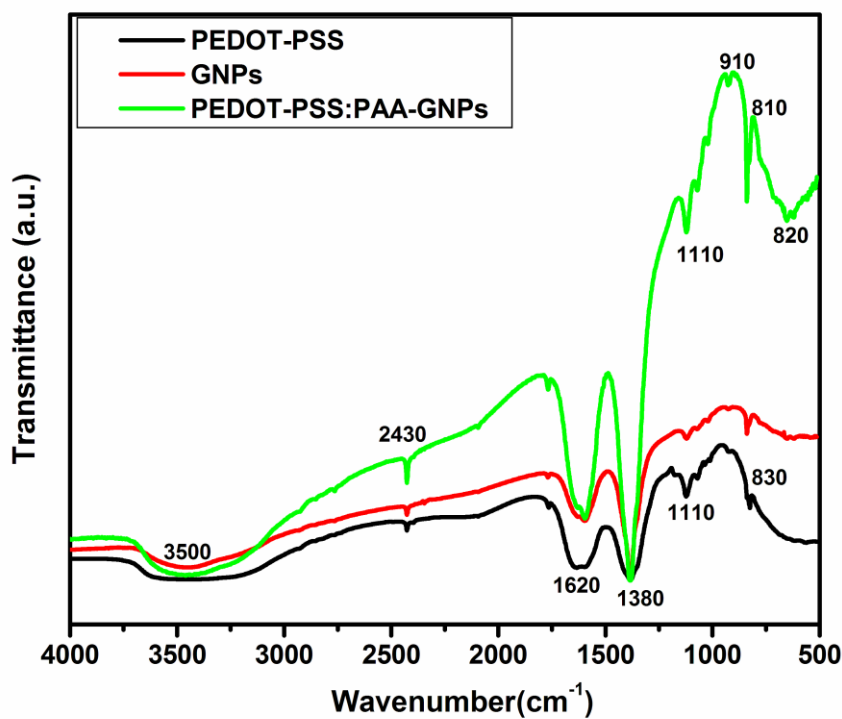


Figure 3. FTIR spectra of (a) bare PEDOT-PSS (b) bare GNPs (c) PEDOT-PSS: PAA-GNPs composite

3.3 Electrical conductivity:

Four probe methods were used to investigate the sheet resistance (R_s) and the temperature dependent electrical conductivity (σ_{dc}) of the samples. In our previous reports, we have demonstrated an effective strategy of secondary doping in PEDOT-PSS films using polar organic polar solvents of high boiling point to improve the conductivity of aqueous PEDOT-PSS dispersions [33, 36-38]. Room temperature conductivity of PEDOT-PSS, PEDOT-PSS treated with PAA and PEDOT-PSS: PAA-GNPs composite is represented in figure-4. The room temperature conductivity of pure PEDOT-PSS enhance from 2 Scm^{-1} to 912 Scm^{-1} in case of PAA treated PEDOT-PSS-GNPs composite films.

The secondary doping of PAA and GNPs presence in PEDOT-PSS matrix significantly improves the conductivity of composite film. The room temperature conductivity of the PEDOT-PSS-GNPs composites treated with PAA shows highest conductivity reported so far in these systems. The secondary doping of PAA in PEDOT-PSS leads to the segregation of phases between conducting rich PEDOT domains and insulating PSS domains, it also helps in partial removal of PSS phase from the polymer matrix. Hence, the PAA doping facilitates the strong interactions between conducting rich PEDOT domains, leads to improved conductivity of the composite films.

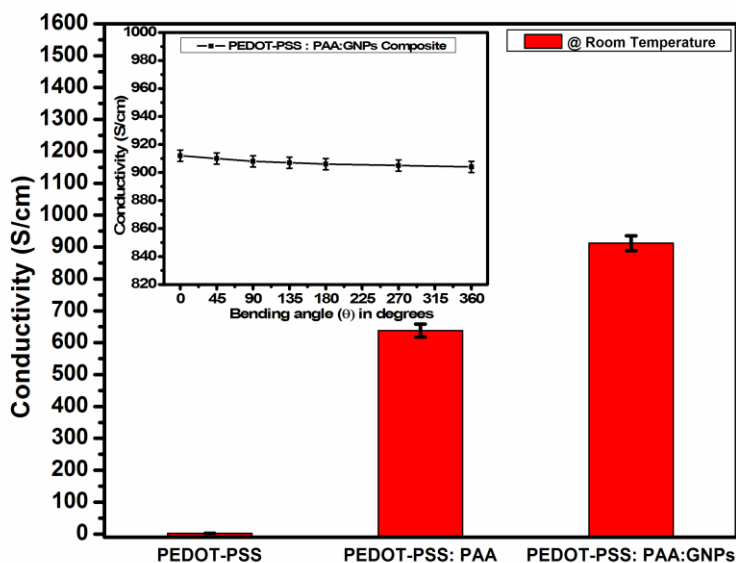


Figure 4. Comparison of conductivities for PEDOT-PSS, PEDOT-PSS: PAA and PEDOT-PSS: PAA:GNPs composite at room temperature (inset: Conductivity of flexible film with bending angles)

Also, the GNPs presence in PEDOT-PSS facilitates π - π interaction and modifies conjugation in the polymer chains which help the creation of de-localized electrons which can easily hop between conducting sites. The combined effect of PAA treatment as well as GNPs presence and their synergetic interactions with PEDOT-PSS enhances the conductivity of composites films. The conductivity enhancement in these hybrid structures of nanocomposite systems can also be attributed to the formation of conducting networks due to the presence of GNPs in PEDOT-PSS matrix. To understand

the flexible nature of these composites for practical applications, electrical conductivity of the composite film is tested at various bending angles, as represented in figure-4 (inset). The PEDOT-PSS: PAA-GNPs composite was subjected to bending angles from 0°-360°. It is interesting to note that the conductivity of the composite films remains almost stable with marginal decrease in their values during the complete cycles of bending (0°-360°). The marginal decrease in conductivity with increasing bending angles may be attributed to reduced strains/tightening up of grain boundaries at the interface, which hinders the charge carrier motion among the polymer chains.

3.4 Electrochemical properties:

The electrochemical properties of the composite electrodes (anodes) were tested using half-cell configurations described in experimental section. Figure-5 shows the C-V characteristics of PEDOT-PSS: PAA-GNPs composite obtained in the potential window of 0 to 3.0 V v/s Li⁺/Li at the scan rate of 0.1 mVs⁻¹. The C-V curves exhibits two reduction peaks at 1.5 and 1.9 V and an oxidation peak at 2.35 V during its cyclic performance. The two reduction peaks observed in the C-V curves are due to long and short chains of Li₂ respectively [39]. The oxidative peak at 2.35 V corresponds to progressive litigation of active material in the presence of electrolyte [40]. The characteristic C-V curves in all the cycles indicate multiple solid-liquid-solid interactions occur between active material and Li. In comparison to 1st cycle of C-V curve, the subsequent 2nd, 3rd, and 4th curves shows much stronger and sharper reduction peaks with a small redox potential gap which indicates the initiation of the activation process of electrodes [41]. After 1st cycle, the curves maintained remarkable repeatable shapes indicating high degree of reversibility during lithiation- delithiation reaction mechanisms. Well overlapping of repeated C-V characteristic peaks shows excellent cycling stability and reversibility of the electrodes. Galvanostatic charge-discharge curves of PEDOT-PSS: PAA-GNPs composites at a constant current density of 200 mAh⁻¹ for different cycles are indicated in figure-6. The PEDOT-PSS: PAA-GNPs composite exhibits initial discharging and charging capacity of ~1280 mAhg⁻¹ and ~1300 mAhg⁻¹ respectively at a constant current density of 200 mAh⁻¹. The contours of all the curves at different cycles exhibit similar behavior with a formation of potential plateaus between 1.75-2.2V for charging and 1-1.4V for discharging corresponds to extraction and insertion of Li⁺ ions respectively. However, the discharge-charge profile declines with repeated cycles which may be due to the fragmentation of anode during cycling, and the formation of a passive solid electrolyte interface (SEI) layer on the fragmented anode surface during the lithiation process [42].

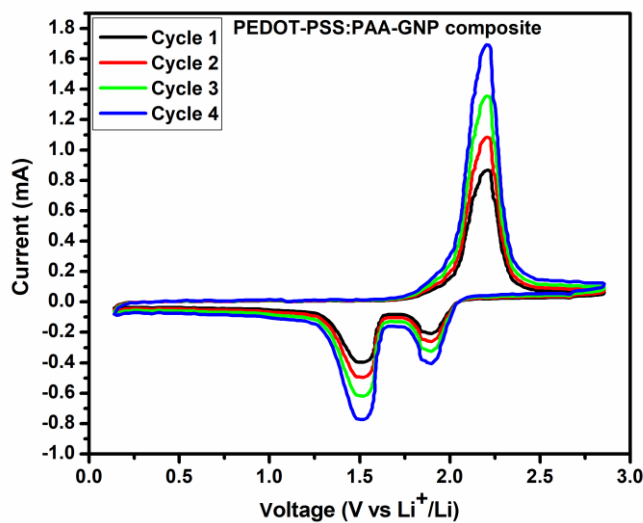


Figure 5. (a) CV curves of PEDOT-PSS: PAA-GNPs composite at different cycles

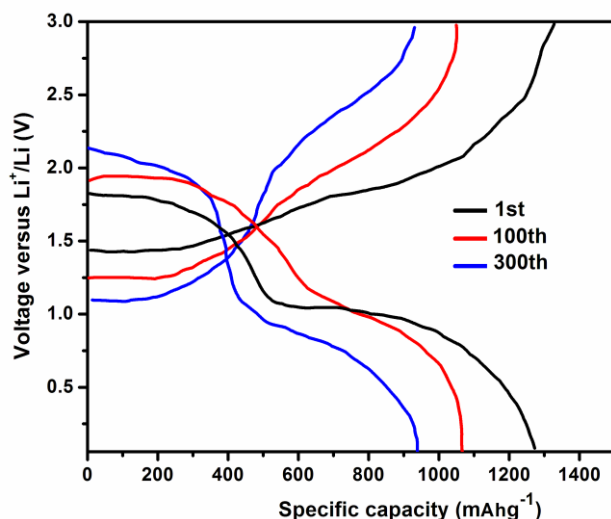


Figure 6. Galvanostatic charge-discharge profiles of PEDOT-PSS: PAA-GNPs composite at different cycles (at a constant current density of 200 mA g^{-1})

The electrochemical performance in terms of specific capacitance of pristine PEDOT-PSS and PEDOT-PSS: PAA-GNPs composites anodes were tested. The dependence of specific capacitance on the GNPs content in PEDOT-PSS treated with PAA is represented in figure-7. The specific capacitance of pristine PEDOT-PSS increased from 796 mAhg^{-1} to 1325 mAhg^{-1} for PEDOT-PSS: PAA-GNPs composite. The observed behavior may be attributed to the formation of excellent conductive channels due to GNPs presence in composite structure that facilitates the electrochemical reaction with the electrolyte in contact. The other reason being increased surface area for the reaction to occur in composite due to addition of GNPs in PEDOT-PSS.

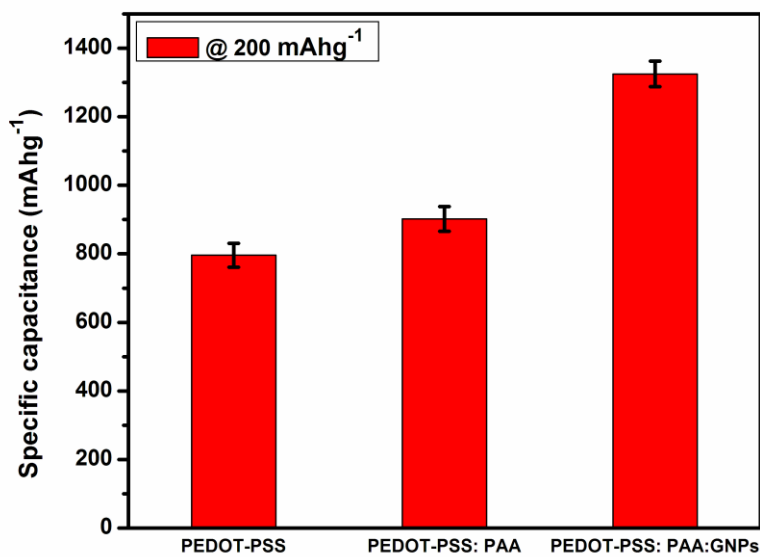


Figure 7. Comparison of specific capacities for PEDOT-PSS, PEDOT-PSS: PAA and PEDOT-PSS: PAA-GNPs composites

The rate performance of bare PEDOT-PSS as well as PEDOT-PSS: PAA-GNPs composite were investigated by cycling at various current densities. As seen in figure-8, the PEDOT-PSS: PAA-GNPs composite exhibit excellent cycle stability for each current density in comparison to bare PEDOT-PSS. The specific capacity of both bare and composite electrodes declines slightly with the increase in rate. However, after testing at the highest current density of 1600 mA g^{-1} , the capacity of the electrode recovers when the current density was reversed to its initial value of 200 mA g^{-1} . These results clearly indicate an excellent high reversibility of the composite anodes. Moreover, the composite anodes shows significant enhancement in the specific capacity in comparison to the bare PEDOT-PSS for different cycles of current densities. The enhanced performance of the composite anodes in comparison to bare PEDOT-PSS may be due to increased porosity in the composite structure. Such porous surface as observed through SEM micrographs is highly advantageous in order to enhance the solid-electrolyte contact. The porous surface with presence of GNPs provides large aspect ratio that provides active sites for absorbing Li ions and facilitates faster electron transfer between electrode-electrolyte interfaces.

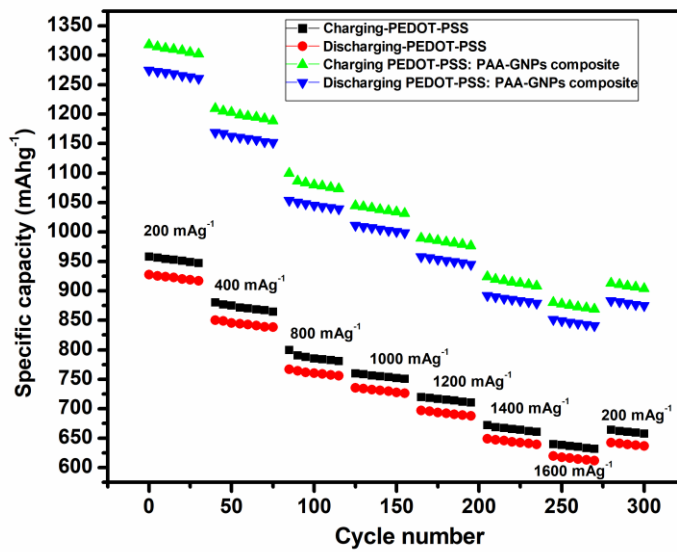


Figure 8. Rate performance of PEDOT-PSS: PAA-GNPs composite for different current densities

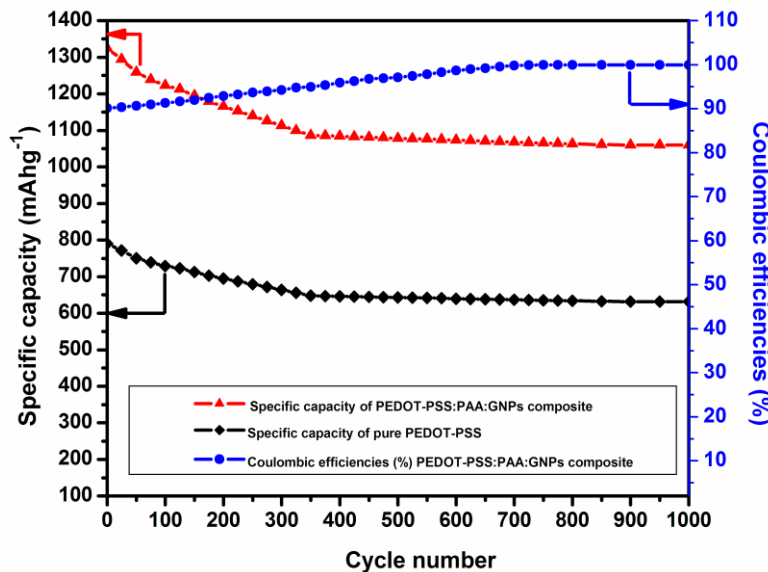


Figure 9. Cyclic performance and the corresponding Coulombic efficiency of bare PEDOT-PSS and PEDOT-PSS: PAA-GNPs composite @ current density 200 mAhg^{-1}

We have further investigated the cyclability of bare PEDOT-PSS as well as PEDOT-PSS: PAA-GNPs (10 wt %) composite anodes up to 1000 cycles at a current density of 200 mAhg^{-1} and the results are depicted in figure-9. It is observed that, PEDOT-PSS: PAA-GNPs composite anodes delivers initial high capacity (1325 mAhg^{-1}) with a small drop in their capacity values up to 350 cycles of operation and becomes almost stable. At the end of 1000 cycles these composite anodes exhibit excellent capacity retention of $\sim 83\%$ with specific capacity of 1102 mAhg^{-1} which are better in comparison to previous reports on PEDOT-PSS based composite anodes [28, 32, 40, 43-49] as

indicated in table-1. On the other hand, capacity of bare PEDOT-PSS reduces from 796 mAhg^{-1} to 640 mAhg^{-1} after 1000 cycles of operation. The composite anodes show an initial coulombic efficiency of 92% which increases gradually with cycles and maintains almost 100% at the end of 1000 cycles of operation.

The kinetics of charge transport in terms of electrons and ions facilitated by bare PEDOT-PSS and PEDOT-PSS: PAA-GNPs composite anodes were investigated through electrochemical impedance spectroscopy (EIS) on the samples after 300 cycles of operation. The EIS in terms of Nyquist plots (figure-10) shows two important characteristic features, in the higher frequency region it comprises of depressed semi-circles followed by inclined straight lines in lower frequency regime. The change in diameters of the semicircles indicates a change in charge transfer resistance (R_{ct}) and an inclined straight line represents a mass transfer process in the electrodes [47]. The R_{ct} of the bare PEDOT-PSS without PAA & GNPs is very high, which is found to decrease with PAA and GNPs inclusion in PEDOT-PSS. The reduction in diameter and area under the curve represents increased conductivity for the composite anodes with content of GNPs in PEDOT-PSS. Also, the inclined line becomes more prominent with the GNPs content in PEDOT-PSS, suggesting the formation of solid-electrolyte-interface due to initiation of activation process in anodes. The charge transfer impedance of bare PEDOT-PSS after 300 cycles of operation is found to be 6680Ω , which decreases to 4980Ω for PAA treated PEDOT-PSS/Graphene nanocomposites. This indicates that the surface modification of conductive PEDOT-PSS using PAA and Graphene improves the electronic conductivity of the composite electrode and reduces its interface and charge transfer impedance.

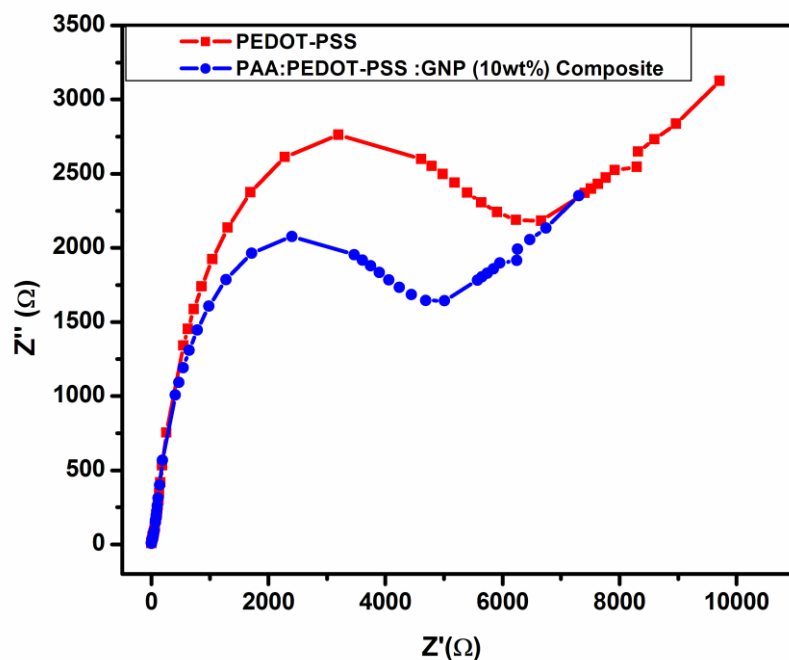


Figure 10. Electrochemical Impedance Spectroscopy (EIS) of bare PEDOT-PSS and PEDOT-PSS: PAA-GNPs composites after 300 cycles of operation @ current density 200 mA g^{-1}

3.5. Effect of PAA and GNPs content on Mechanical properties of PEDOT-PSS

Mechanical properties of the bare PEDOT-PSS, PVA treated PEDOT-PSS and PEDOT-PSS: PAA-GNPs composite films in terms of stress-strain behavior, Young's modulus and tensile strength were investigated. Figure-11 shows the variation of stress-strain curves for the three samples, which demonstrates improved mechanical properties due to PAA treatment and GNPs addition in PEDOT-PSS. The PAA treatment followed by GNPs addition in PEDOT-PSS has resulted into large strains in the composite samples. Figure-12 represents the effect of PAA treatment and GNPs addition on Young's modulus as well as Tensile strength of PEDOT-PSS films. It is interesting to see that, both the Young's modulus as well as tensile strength of the bare PEDOT-PSS increases from 2.4 ± 0.2 GPa to 3.7 ± 0.2 GPa and 55 ± 2.5 MPa to 67 ± 2.5 MPa respectively, upon PAA treatment. Further, both Young's modulus as well as tensile strength of the composite films enhances to 4.6 ± 0.2 GPa and 78 ± 2.5 GPa respectively upon addition of GNPs in PAA treated PEDOT-PSS. The improved mechanical properties of the composites are due to good dispersion of PAA and GNPs in PEDOT-PSS. The hydrogen bonding between reinforced PAA and PEDOT-PSS matrix could be one of the factors for the improved mechanical properties of PAA: PEDOT-PSS films. The plate-like-morphologies of GNPs could be another interesting structural feature that further enhances the Young's modulus and tensile strength of the composites. Hence, presence of PAA and GNPs results into hybrid chemical cross-links and hydrogen bonding interactions in PEDOT-PSS networks endow PEDOT-PSS: PAA-GNPs composites with excellent mechanical properties.

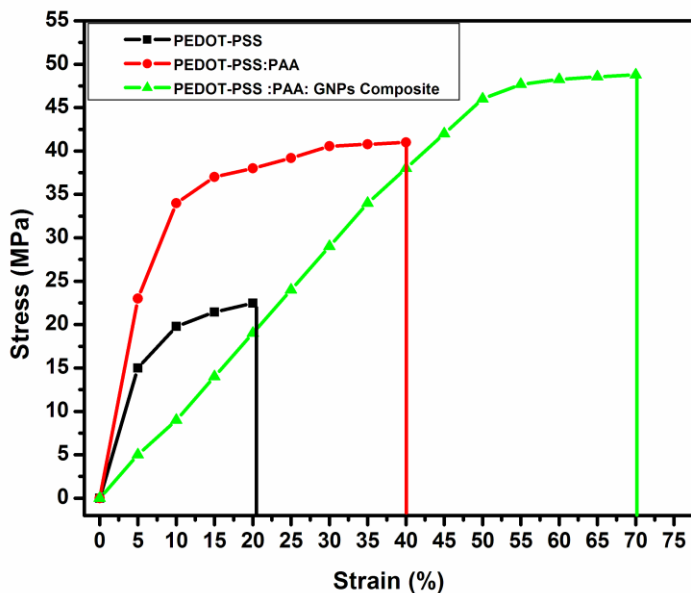


Figure 11. Stress-Strain variation for PEDOT-PSS, PEDOT-PSS: PAA and PEDOT-PSS: PAA-GNPs composite

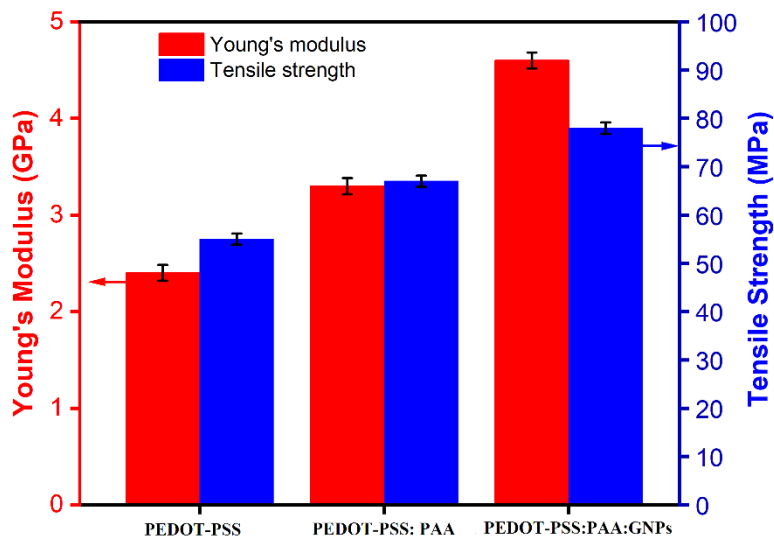


Figure 12. Young's modulus and tensile strength tests for PEDOT-PSS, PEDOT-PSS: PAA and PEDOT-PSS: PAA-GNPs composite

Table 1. PEDOT-PSS based composite active anode materials, synthesis method and electrochemical performances

Active material used as a composite	Synthesis method	Conductivity S/cm	Mechanical Properties (Young's modulus, tensile strength)	Electrochemical properties initial specific capacity (mAhg ⁻¹)	Electrochemical properties Cycles (Capacity retention)	Reference
PEDOT-PSS-Graphene	Surface coating	Not reported	Not reported	1000	200 (1000 mAhg ⁻¹)	28
MoS ₂ / PEDOT:PSS	Dip coating	Not reported	Not reported	712	100 (81%)	32
PEDOT-PSS-Ge	Vapor Deposition	Not reported	Not reported	1800	200 (50%)	40
PEDOT-PSS/Ge/CuO	Spin Coating	Not reported	Not reported	980	1000 (90%)	43
NaCa ₂ Si ₃ O ₈ (OH)/PEDOT:PSS	One step hydrothermal method	Not reported	Not reported	300	50 (100 mAhg ⁻¹)	44
MnO ₂ /PEDOT-PSS	Sonication	Not reported	Not reported	800	200 (1450 mAhg ⁻¹)	45
nano-Sn/PEDOT:PSS/PVA CSHC	In-situ polymerization	Not reported	Not reported	800	200 (72%)	46
PEDOT:PSS SnO ₂ /reduced graphene oxide	In-situ polymerization	Not reported	Not reported	1759	100 (851 mAhg ⁻¹)	47
PEDOT:PSS@Ge	Solution impregnation method	Not reported	Not reported	1450	200 (57.4%)	48
Si/PEDOT:PSS	In-situ polymerization	Not reported	Not reported	1096	200 (60.58%)	49
PEDOT-PSS/Graphene Nanoplatelets treated with PAA	Bar coating	912	4.6 GPa, 78 GPa	1325	1000 (1100 mAhg ⁻¹)	Present work

In this work, PEDOT-PSS: PAA-GNPs composites were prepared by simple bar coating technique, which is cost-effective, flexible, and suitable for large scale production of electrodes. The improved electrochemical performance of these composite systems resulting due to unique

microstructure, large surface area, porosity, and conductive networks facilitate the lithium reactions. Due to excellent conductivity, electrochemical performance, and mechanical flexibility, these nanocomposite anodes are potential materials for future generation flexible LIBs for wearable electronic devices.

4. CONCLUSIONS

We have successfully fabricated and tested a free-standing, flexible, and robust composite film as an anode for Li-Ion batteries (LIBs) using simple strategies. Utilizing the advantages of higher theoretical capacity of GNPs, excellent electrical conductivity and mechanical flexibility of PEDOT-PSS, we have developed an efficient strategy to fabricate PEDOT-PSS: PAA- GNPs composites anode with enhanced electrochemical performance as an electrode in LIBs. The GNPs presence in PEDOT-PSS significantly enhances the conductivity from 2 Scm^{-1} to 912 Scm^{-1} for PEDOT-PSS: PAA-GNPs composite. The representative anodes of PEDOT-PSS: PAA-GNPs composite shows improved rate performance and excellent cyclic stability. It renders a specific capacity of 1102 mAhg^{-1} after 1000 cycles at a constant current density of 200 mA g^{-1} . Moreover, the composite anode shows a capacity retention of ~83% and coulombic efficiency of ~99% after 1000 cycles. The composite film with ultimate electrochemical performance shows an improved Young's modulus of $2.4 \pm 0.18 \text{ GPa}$ to $4.6 \pm 0.18 \text{ GPa}$ and Tensile strength of $55 \pm 2.5 \text{ MPa}$ to $78 \pm 2.5 \text{ MPa}$ in comparison to pure PEDOT-PSS films. We anticipate that this simple and scalable approach to fabricate electrodes for LIBs will provide platform for the development of low cost graphene based flexible, robust electrodes with excellent electrochemical performance.

ACKNOWLEDGEMENTS

Authors SK & NB acknowledge the financial support towards this research from Deanship of Scientific Research (DSR), University of Tabuk, Tabuk, Saudi Arabia, under research Grant No.S-1440-0177.

DECLARATION OF INTEREST

Authors listed in the manuscript certify that they have NO affiliations with or involvement in any organization or entity with any financial interest or non-financial interest in the subject matter or materials discussed in this manuscript.

References

1. Yue Wang, Chenxin Zhu, Raphael P fattner, Hongping Yan, Lihua Jin, Shucheng Chen, Francisco Molina-Lopez, Franziska Lissel, Jia Liu, Noelle I. Rabiah, Zheng Chen, Jong Won Chung, Christian Linder, Michael F. Toney, Boris Murmann and Zhenan Bao, *Sci.Adv.*, 3 (2017) e1602076.
2. G.H. Yu, X. Pan , L.J. Bao and Z.N. Cui, *Nano Energy.*, 2 (2013) 213.
3. M.D. Dickey, *J. Adv. Mater.*, 29 (2017) 1606425.

4. J. Yun, C. Song, H. Lee, H. Park, Y.R. Jeong, J.W. Kim, S.W. Jin, S.Y. Oh, L.F. Sun and G.Zi, *Nano Energy.*, 49 (2018) 644.
5. H. Souri and D. Bhattacharyya, *ACS Appl. Mater. Interfaces.*, 10 (2018) 20845.
6. J. Pu, X.H. Wang, R. Xu and K. Komvopoulos, *ACS Nano.*, 10 (2016) 9306.
7. S. Gong and W.L. Cheng, *Adv. Energy Mater.*, 7 (2017) 1700648.
8. H.S. Li, Y. Ding, H. Ha, Y. Shi, L.L. Peng, X.G. Zhang, C.J. Ellison and G.H. Yu, *J. Adv. Mater.*, 29 (2017) 1700898.
9. Y. Shi, L.L. Peng, Y. Ding, Y. Zhao and G.H Yu, *Chem. Soc. Rev.*, 44 (2015) 6684.
10. Y. Shi, L.L. Peng and G.H. Yu, *Nanoscale.*, 7 (2015) 12796.
11. Y.Z. Xie, Y. Liu, Y.D. Zhao, Y.H. Tsang, S.P. Lau, H.T. Huang and Y. Chai, *J. Mater. Chem. A*, 2 (2014) 9142.
12. H.Y. Jin, L.M. Zhou, C.L. Mak, H.T. Huang, W.M. Tang and H.L. Chan, *Nano Energy.*, 11 (2015) 662.
13. X.B. Zang, M. Zhu, X. Li, X.M. Li, Z. Zhen, J.C. Lao, K.L. Wang, F.Y. Kang, B.Q. Wei and H.W. Zhu, *Nano Energy.*, 15 (2015) 83.
14. K. Guo, X.F. Wang, L.T. Hu, T.Y. Zhai, H.Q. Li and N. Yu, *ACS Appl. Mater. Interfaces.*, 10 (2018) 19820.
15. P.Li, P.Jin, Z.Y.Peng L.L.Zhao ,F.D.Xiao Jin and G.H.Yu, *Adv. Mater.*, 30 (2018) 1800124.
16. R. Qi, J. Nie , J.H. Liu , M.Y. Xia and M.Y. Lu , *Nanoscale.*, 10 (2018) 7719.
17. S.L. Wang, N.S. Liu, J. Su, L.Y. Li, F. Long, Z.G. Zou, X.L. Jiang and Y.H. Gao, *ACS Nano.*, 11 (2017) 2066.
18. K. Lota, V. Khomenko and E. Frackowiak, *J. Phys. Chem. Solids.*, 65 (2004) 295.
19. Y. Shi, L.L. Peng, Y. Ding, Y. Zhao and G.H. Yu , *J. Chemistry Society Review.*, 44 (2015) 6684.
20. L. Wen, F. Li and H.M. Cheng, *J. Adv. Mater.*, 28 (2016) 4306.
21. H. Bai, C. Li, and G. Shi, *J. Adv. Mater.*, 23 (2011) 1089.
22. Z.S. Wu, G.M. Zhou, L.C. Yin, W. Ren, F. Li and H.M. Cheng, *Nano Energy.*, 1 (2012) 107.
23. C.H. Xu , B.H. Xu, Y.Gu, Z.G. Xiong, J. Sun and X.S. Zhao, *Energy Environ. Sci.*, 6 (2013) 1388.
24. Brian D. Adams, Claudio Radtke, Robert Black, Michel L. Trudeau, Karim Zaghib and Linda F. Nazar, *Energy Environ. Sci.*, 6 (2013) 1772.
25. Betar M. Gallant, David G. Kwabi, Robert R. Mitchell, Jigang Zhou, Carl V. Thompson and Yang Shao-Horn, *Energy Environ. Sci.*, 6 (2013) 2518.
26. Betar M. Gallant, Robert R. Mitchell, David G. Kwabi, Jigang Zhou, Lucia Zuin, Carl V. Thompson and Yang Shao-Horn, *J. Phys. Chem. C*, 116 (2012) 20800.
27. M.M. Thotiyil, S.A. Freunberger, Z. Peng and P.G. Bruce, *J. Am. Chem. Soc.*, 135 (2013) 494.
28. Dae Ho Yoon, Seon Hye Yoon, Kwang-Sun Ryu and Yong Joon Park, *Sci. Rep.*, 6 (2016) 19962
29. Jin Pan, Guiyin Xu, Bing Ding, Zhi Chang, Aixiu Wang, Hui Dou and Xiaogang Zhang, *RSC Adv.*, 6 (2016) 40650.
30. J.A. Li, J.C. Liu and C.J. Gao, *J. Polym. Res.*, 17 (2010) 713.
31. Bettina Friedel, Panagiotis E. Keivanidis, Thomas J. K. Brenner, Agnese Abrusci, Christopher R. McNeill, Richard H. Friend, and Neil C. Greenham, *Macromolecules.*, 42 (2009) 6741.
32. X. Zhao, Y. Mai, H. Luo, D. Tang, B. Lee, C. Huang, L. Zhang, *Appl. Surf. Sci.*, 288 (2014) 736.
33. Syed Khasim, Apsar Pasha, Nacer Badi, Mohana Lakshmi and Yogendra Kumar Misra, *RSC Adv.*, 10 (2020) 10539.
34. P.L. Anto, C.Y. Panicker and H.T. Varghese Philip, *J. Raman Spectrosc.*, 37(2006), 1265.
35. Z. Wang, B. Huang, Y. Dai, Y. Liu, X. Zhang, X. Qin, J. Wang, Z. Zheng and H. Cheng, *CrystEngComm.*, 14(5) (2012) 1692.
36. Syed Khasim, Apsar Pasha, Aashish S Roy, Ameena Parveen, and Nacer Badi, *J. Electron. Mater.*, 46 (7):(2017),4447
37. Apsar Pasha and Syed Khasim, *J. Mater. Sci. - Mater. Electron.*, 31 (2020) 9185.

38. Apsar Pasha, Syed Khasim, Faheem Ahmad Khan and N. Dhananjay, *Iran. Polym. J.*, 28 (2019) 183.
39. Yu-Sheng Su, Yongzhu Fu, Thomas Cochell, and Arumugam Manthiram, *Nat. Commun.*, 4 (2013) 2985.
40. Jian Hao, Lei Pan, Hangchuan Zhang, Caixia Chi, Qingjie Guo, Jiupeng Zhao, Yu Yang, Xiaoxu Liu, Xiaoxuan Ma and Yao Li , *Chem. Eng. J.*, 346 (2018) 427.
41. W. Li, G. Zheng, Y.Yang , Z.W Seh, N. Liu and Y. Cui , *Proc. Natl. Acad. Sci. U.S.A.*, 110 (2013) 7153.
42. W. He, H.J. Tian , X.L. Wang, F.X. Xin and W.Q. Han, *J. Mater. Chem. A*, 3 (2015) 19393.
43. Shuai Bai, Yaodong Ma, Xinyu Jiang, Qun Li, Zhibo Yang, Qiming Liu and Deyan He, *Surf. Interfaces.*, 8 (2017) 214.
44. Shaoyan Zhang, Lijie Ci, Wei Mu and Min Lu, *Chem. Phys. Lett.*, 715 (2019) 40.
45. In-Hwan Ko, Seong-Jun Kim, Joohyun Lim, Seung-Ho Yu, Jihoon Ahn, Jin-Kyu Lee and Yung-Eun Sung, *Electrochim. Acta.*, 187 (2016) 340.
46. Daqian Ma, Peng Bi, Haowen Meng, Xiaohui Yu, Peng Dou, Hongyan Yang, Yanli Sun, Zhenzhen Cao, Jiao Zheng, Chao Wang, Xinhua Xu, *J. Mater. Sci. - Mater. Electron.*, 26 (2015) 7523
47. Md. Selim Arif Sher Shah, Shoaib Muhammad, Jong Hyeok Park, Won-Sub Yoon and Pil J. Yoo, *RSC Adv.*, 5 (2015) 13964
48. Jinfeng Liu, Jing Xu , Yufang Chen, Weiwei Sun, Xiaoxiong Zhou, Jianhuang Ke, *Int. J. Electrochem. Sci.*, 14 (2019) 359
49. L. Yue, S. Wang, X. Zhao, L. Zhang, *J. Mater. Chem.*, 22 (2012) 1094.
50. Zhiyu Wang, Jianli Cheng,Wei Ni, Lizhen Gao, Dan Yang, Joselito M. Razal and Bin Wang, *J. Power Sources*, 342 (2017) 772.

© 2021 The Authors. Published by ESG (www.electrochemsci.org). This article is an open access article distributed under the terms and conditions of the Creative Commons Attribution license (<http://creativecommons.org/licenses/by/4.0/>).